AUTHOR	Tuncer Turker, Ozyurt Fatih, Dogan Sengul, Subasi Abdulhamit
TITLE	A novel Covid-19 and Pneumonia Classification Method based on F-transform
YEAR	2021
DOI	10.1016/j.chemolab.2021.104256
VERSION	Author's accepted manuscript
CITATION	Turker Tuncer, Fatih Ozyurt, Sengul Dogan, Abdulhamit Subasi, A novel Covid-19 and pneumonia classification method based on F-transform, Chemometrics and Intelligent Laboratory Systems, Volume 210, 2021, 104256, ISSN 0169-7439, https://doi.org/10.1016/j.chemolab.2021.104256

A novel Covid-19 and Pneumonia Classification Method based on F-transform

Turker TUNCER
Department of Digital Forensics Engineering, Firat University
Elazig, 23000, Turkey
turkertuncer@firat.edu.tr
ORCID
0000-0002-1425-4664

Fatih OZYURT
Department of Software Engineering, Firat University
Elazig, 23000, Turkey
fatihozyurt@firat.edu.tr
ORCID
0000-0002-8154-6691

Sengul DOGAN
Department of Digital Forensics Engineering, Firat University
Elazig,23000, Turkey
sdogan@firat.edu.tr
ORCID
0000-0001-9677-5684

Abdulhamit SUBASI
Institute of Biomedicine, Faculty of Medicine, University of Turku, 20520, Turku, Finland.
E-mail: abdulhamit.subasi@utu.fi
Department of Computer Science, College of Engineering, Effat University, Jeddah, 21478, Saudi Arabia.
E-mail: absubasi@effatuniversity.edu.sa
ORCID
0000-0001-7630-4084

Abstract:
Nowadays, Covid-19 is the most important disease that affects daily life globally. Therefore, many methods are offered to fight against Covid-19. In this paper, a novel fuzzy tree classification approach was introduced for Covid-19 detection. Since Covid-19 disease is similar to pneumonia, three classes of data sets such as Covid-19, pneumonia, and normal chest x-ray images were employed in this study. A novel machine learning model, which is called the exemplar model, is presented by using this dataset. Firstly, fuzzy tree transformation is applied to each used chest image, and 15 images (3-level F-tree is constructed in this work) are

obtained from a chest image. Then exemplar division is applied to these images. A multi-kernel local binary pattern (MKLBP) is applied to each exemplar and image to generate features. Most valuable features are selected using the iterative neighborhood component (INCA) feature selector. INCA selects the most distinctive 616 features, and these features are forwarded to 16 conventional classifiers in five groups. These groups are decision tree (DT), linear discriminant (LD), support vector machine (SVM), ensemble, and k-nearest neighbor (k-NN). The best-resulted classifier is Cubic SVM, and it achieved 97.01% classification accuracy for this dataset.

Keywords: Corona; Covid-19; Fuzzy tree; multi-kernel local binary pattern; texture recognition; X-ray image recognition.

1. Introduction

COVID-19 is a virus that transmits from person to person and affects the whole world. This virus, which causes deaths, originally arose in Wuhan, China. However, it later spread to 209 countries [1, 2]. The Covid-19 virus is a member of the coronavirus family and is a newly encountered virus, and our body is unable to react because it is not recognized by the human immune system [3]. The virus most often settled in the lungs and multiplies there. Severe respiratory distress indicates because of this virus. For this reason, people face respiratory distress [4].

There are varieties of coronaviruses. The source of these viruses has been identified as musk cats in the acute respiratory syndrome (SARS) outbreak and as the dromedary camel in the middle east respiratory syndrome (MERS) outbreak [5-7]. In the Covid-19 epidemic, the source has not yet been identified. However, its genetic sequence is thought to be bat-derived. Its rapid spreading is an indication that this virus has been transmitted from person to person. In order to prevent the spreading of further Covid-19 virus, countries have blocked international exits [8-11]. At the same time, curfews have been announced within many countries. It is aimed to reduce the transmission rate of the covid-19 virus in countries where going out and contact are reduced as much as possible [12-14]. This virus's common symptoms include high fever, difficulty breathing, dry cough, fatigue, decreased taste, and smell. In this case, it causes lesions and pneumonia in the lungs. This disease can result in death in the later stages [15, 16].

Many studies have been carried out on machine learning and artificial intelligence in the literature [17-21]. Some of these studies have been conducted on disease diagnosis [20, 22, 23]. In this study, a method for diagnosing Covid-19 disease using the Fuzzy tree and multi-kernel local binary pattern is proposed. Details of the proposed method are presented in the sections below.

1.1 Motivation

Nowadays, the Covid-19 virus affected all humans in the world. The Covid-19 disease is similar to pneumonia. Our main objective is to differentiate Covid-19 patients from pneumonia patients. Therefore, novel textural features and fuzzy transform-based automated chest images classification method were presented.

Several studies are presented in the literature on Covid-19 and Pneumonia disease. Narin et al. [24] proposed a hybrid method, which used ResNet50, InceptionV3, and Inception-ResNetV2 convolutional neural network (CNN) architecture to classify normal chest images and chest images with Covid-19 diagnosis [25]. They achieved a 98.0% accuracy rate for two classes. Jaiswal et al. [26] used Mask-RCNN based model that improved the ResNet101 and ResNet50. They obtained a 99.1% precision value by using NIH CXR14 [27] dataset. Sethy and Behera [28] used the CNN model to classify *two* classes, and they succeeded 95.38% accuracy rate. Xu et al. [29] used two CNN three-dimensional classification models for two classes of chest images. They obtained 86.7% accuracy with collected data of 2 classes. Wang et al. [30] collected 325 CT images of COVID-19 and 325 CT images. They obtained an 89.5% success rate by using the inception transfer-learning model. Sirazitdinov et al. [31] used an ensemble of two CNN. They utilized the available RSNA Pneumonia Detection Challenge dataset [32] and obtained 79.3% recall rates. Liang and Zheng [33] presented a residual structure for the classification of pediatric pneumonia images. They used the Kermany dataset [34] with 5856 chest X-ray images collected and tagged from children. They achieved a 96.7% accuracy performance rate. Rajpurkar et al. [35] improve a method that can detect pneumonia from chest X-ray images. Their proposed CheXNet method is a 121-layer CNN trained on the ChestX-ray14 database [27] obtained 93.71% value. Ghoshal and Tucker [36] investigated how Dropweights based Bayesian CNN (BCNN) can estimate uncertainty in Deep Learning solutions to develop the diagnostic performance of the human-machine combination using publicly available COVID-19 chest X-ray dataset [37]. Pham [38] suggested a method to diagnose Covid-19 disease using X-ray images. These images are evaluated using convolutional neural networks method. Sallay et al. [39] proposed an approach for Covid-19 disease detection using machine learning techniques. CT and X-ray images were used for different databases in the study. Moreover, the average accuracy value was calculated as 82.88%. Sun et al. [40] proposed a method for diagnosing Covid-19 disease, where Adaptive Feature Selection guided Deep Forest was utilized with 1495 Covid-19 and 1027 pneumonia patients data. Accuracy rate of these data was calculated as 91.79%.

1.2 Novelties and Contributions

In this article, a novel exemplar chest image classification method was proposed using the proposed F-transform and MKLBP. The novelties are;

- A lightweight multileveled feature extraction method is developed. In this method, a fuzzy transform (F-transform) [41] based on triangle fuzzy sets is proposed and a novel fuzzy tree is constructed using the triangle-based F-transform.
- As we know from literature, F-transforms have been used for image and noise reduction [42]. The proposed fuzzy tree is utilized as a novel operator like convolution.
- Signum and ternary kernels are utilized together to generate features comprehensively because local image descriptor has high performance for feature extraction.
- Highly accurate chest image classification method is developed for Covid-19 detection with a classification rate of 97.01%.

Contributions of this study are;

- In the computer vision applications, discrete wavelet transform, Gabor filters based decomposition, or pooling methods are utilized for decomposition. In order to recommend an effective decomposition model, a new fuzzy tree-based decomposer is presented and successful results have been attained by using this transform.
- Hand-crafted feature generation methods are effective, and they have low computational complexity. Moreover, the implementation of them is easy. However, they cannot solve some computer vision problems since they extract low-level features. Multilayer/multilevel feature generation methods must be created to increase the strength of the hand-crafted feature generators. A multilevel feature generator using the presented fuzzy tree decomposition and multiple kernel local binary pattern is utilized to extract both high-level and low-level features. Further, INCA [43] is utilized as feature selector to choose the optimum number of features for this problem. By using these basic and effective methods, a highly accurate Covid-19 detection method with a short execution time is presented.

2. Backgrounds

The proposed method uses F-transform and MKLBP, which are explained in this section.

2.1 Fuzzy Transform (FT)

One of the most efficient methods for image reduction is the fuzzy transform. Martino et al. [42] proposed a concept of fuzzy transform for color image reduction. The image is divided into m x n sizes of non-overlapping blocks to perform this transform. Then, the membership degree of each pixel is calculated. Finally, Eq. 1 is used for reduction.

$$F_{r,c} = \frac{\sum_{i=1}^{m}\sum_{j=1}^{n}\frac{pv_{i,j}}{255}A_{r,i}B_{c,j}}{\sum_{i=1}^{m}\sum_{j=1}^{n}A_{r,i}B_{c,j}} \quad (1)$$

where pv defines pixel values of the image, F is fuzzy value, A and B are membership degrees of the pixel values.

Inverse fuzzy transform is described in Eq. 2 [42].

$$pv_{i,j}^{F} = \sum_{i=1}^{m}\sum_{j=1}^{n}F_{r,c}A_{r,i}B_{c,j} \quad (2)$$

In this paper, a novel FT is presented for image reduction. In the presented method, triangle fuzzy sets are selected for image reduction, and this method is explained in Section 3.

2.2 Multi Kernel Local Binary Pattern

MKLBP is an improved version of the LBP [44] and LTP [45]. LBP and LTP use 3 x 3 sized overlapping blocks and the same pattern. The main difference between these feature extractors is the used kernel (binary feature generation) function. While LBP uses the signum function as the kernel, LTP uses the ternary function. Equations of function are given in Eqs 3-4.

$$s(P_C, P_L) = \begin{cases} 0, P_C - P_L < 0 \\ 1, P_C - P_L \geq 0 \end{cases}, L = \{1,2,\dots,8\} \quad (3)$$

$$t(P_C, P_L, d) = \begin{cases} 1, P_C - P_L > d \\ 0, |P_L - P_C| < d \\ -1, P_L - P_C < -d \end{cases} \quad (4)$$

where s(.,.) and t(.,.,.) define signum and ternary functions respectively. PC is the center pixel of the 3 x 3 sizes block, PLs are neighbor pixels of the center pixel, d represents threshold value, and generally, this value is user-defined. Eqs. 5-6 define bit extraction from ternary value.

$$bit^{lower} = \begin{cases} 0, t > -1 \\ 1, t = -1 \end{cases} \quad (5)$$

$$bit^{upper} = \begin{cases} 0, t < 1 \\ 1, t = 1 \end{cases} \quad (6)$$

By using the extracted upper and lower bits, upper and lower feature images are created. The Signum function generates 8 bits, and the ternary function generates 16 bits, 8 bits upper and 8 of the lower. Therefore, the proposed MKLBP generates *three* feature images named signum, upper and lower. The length of the histogram of each image is 256. Hence, MKLBP generates 768 features. The procedure of the MKLBP is shown in Fig. 1.

Procedure: $MKLBP(Im)$

Input: Image (Im) with size of W x H. Threshold value (thr)

Output: Feature vector (fv) with length of 768.

01: **for** i=1 to W-2 **do**
02: **for** j=1 to H-2 **do**
03: $blk = Im(i{:}i+2)$; // Block division
04: $signum(i,j) = 0;\ upper(i,j) = 0;\ lower(i,j) = 0;$ // Assign 0 to first values.
05: $cnt = 1;$
06: **for** m=1 to 3 **do**
07: **for** n=1 to 3 **do**
08: **if** m! =2 || n! =2 **then** // Skip center pixel
09: $signum(i) = signum(i) + \big(blk(m,n) \geq blk(2,2)\big) * 2^{8-cnt};$
10: $upper(i) = upper(i) + \big(blk(m,n) - blk(2,2)\big) > thr * 2^{8-cnt};$
11: $lower(i) = lower(i) + \big(blk(m,n) - blk(2,2)\big) < -thr * 2^{8-cnt};$
12: $cnt++;$
13: **end if**
14: **end for n**
15: **end for m**
16: **end for j**
17: **end for i**
18: Generate histogram of the calculated *signum*, *upper* and *lower* signals
19: Concatenate histograms and obtain fv

Fig. 1. MKLBP procedure

As seen from the procedure, lines 09-11 extract binary features, and these binary features are converted to decimal values in these lines. Histogram extraction is given in line 18. A mathematical description of the histogram extraction is indicated below.

$$histogram = zeros(1{,}256) \tag{7}$$

$$histogram\big(value(i,j)\big) + +, i = \{1{,}2, \dots, W-2\}, j = \{1{,}2, \dots, H-2\} \tag{8}$$

A graphical demonstration of the MKLBP method is given in Fig. 2.

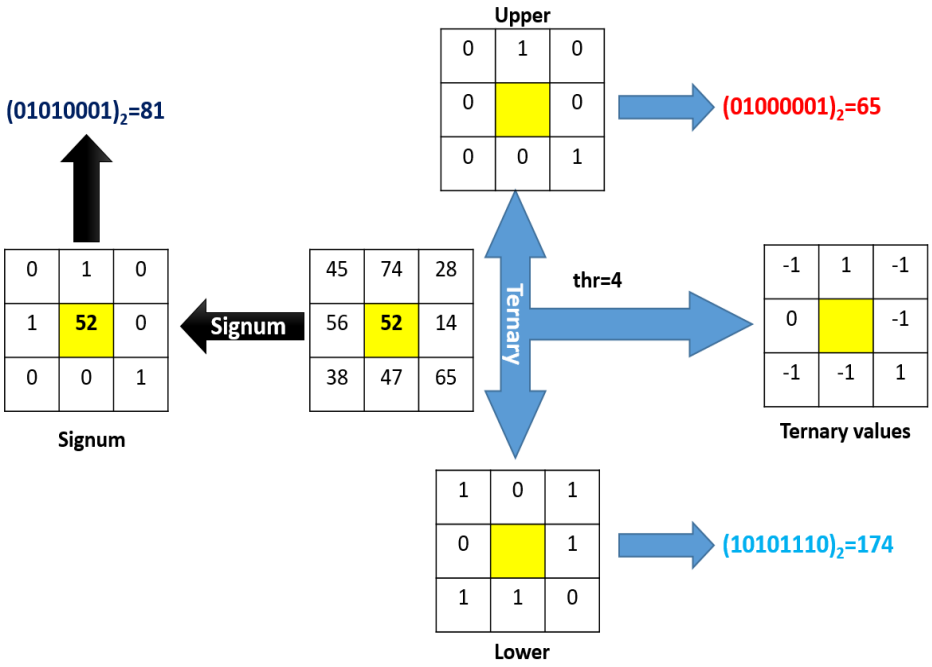

Fig. 2. Graphical demonstration of an example about MKLBP

3. Material

There may be some rules that cannot be well found by the less experienced doctor's eye on the X-ray images. Chest X-ray images of patients infected with COVID-19 are just one of these images. In COVID-19 patients, chest X-ray images show mostly bilateral involvement abnormalities [46].

3.1 Dataset

In this study, chest X-ray images were used to detect the COVID-19. The used database is composed of the publicly available datasets. 135 X-ray images with COVID-19 diseases were collected from GitHub [47]. 46 of these patients are female, and 64 are male, and 25 of them are not determined. While 17 patients were between 25 and 49 years old, 118 patients were over 50 years old. To increase the reliability of the proposed method, normal and pneumonia diagnosis images were downloaded from the Kaggle platform. Due to the scarcity of COVID-19 diagnosed X-ray images, only 150 normal and pneumonia chest X-ray images were selected from Kaggle [48]. Posterior anterior (PA) images were chosen to increase the visibility of the spotting. Our experiments are based on a data set of 135 COVID-19, 150 pneumonia patients and 150 normal (total 435 images) chest x-ray images. In Figure 3, COVID-19, normal, and pneumonia patient's chest X-ray images are presented.

a) X-ray images of chest diagnosed as COVID-19

b) X-ray images of chest diagnosed as Pneumonia

c) X-ray images of chest diagnosed as healthy

Fig. 3. Representation of chest x-ray images

4. The proposed image classification method

A novel chest image classification method is implemented by using the proposed F-transform and MKLB. The stages of this method are given below.

- Feature extraction
- Feature selection
- Classification.

A graphical outline of this method is presented in Fig. 4.

In Fig. 4, the graphical presentation of the proposed fuzzy MKLBP and INCA based method is shown. The novelties of the proposed method are the utilization of the fuzzy tree and INCA feature selection approach. By using the fuzzy tree, a multilevel feature extraction method is created. In this work, MKLBP is utilized for feature extraction and INCA is chosen for feature selection. In the classification phase, 16 classifiers are used to show the general success of the proposed exemplar MKLBP and INCA based feature extraction and feature selection.

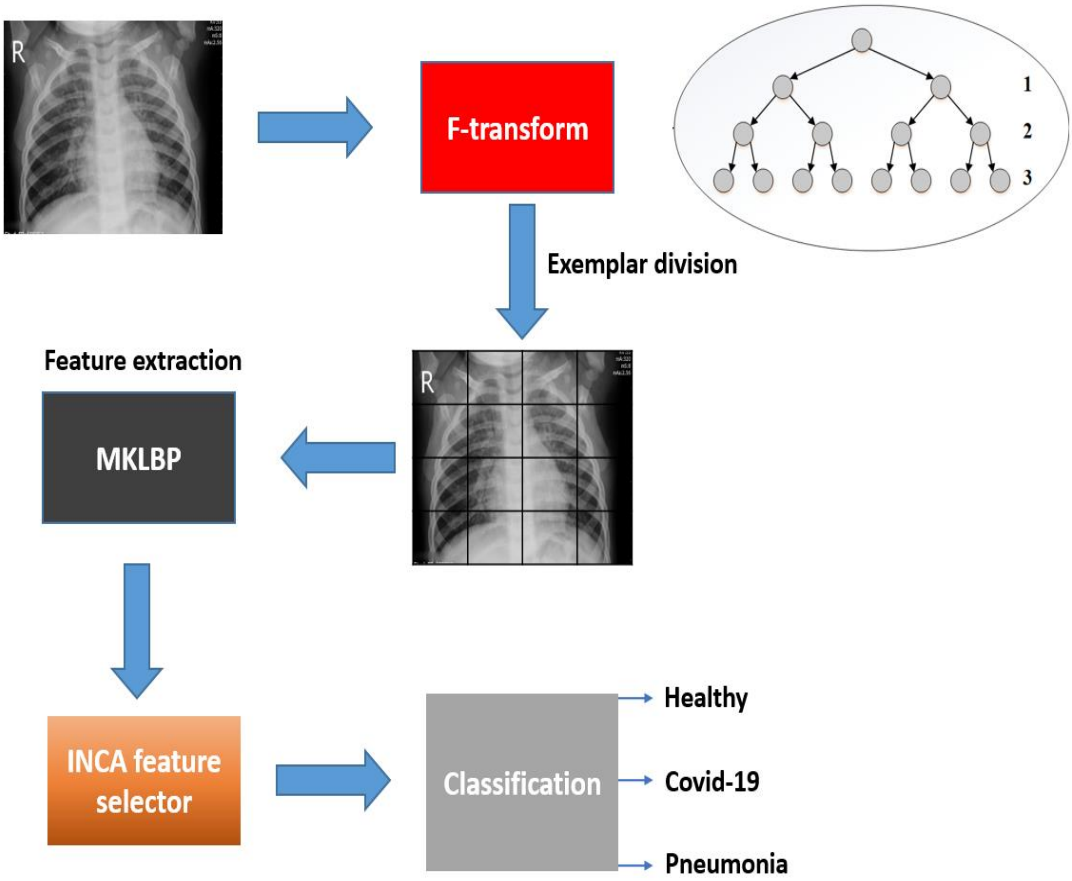

Fig. 4. Graphical outline of the F-transform, MKLBP, and INCA based chest image classification method

The steps of this method are given below.

Step 1: Load image.

Step 2: Create a fuzzy tree. Triangle F-transform is proposed to create this tree. The steps of the triangle F-transform method given below.

In this article, *three* levels of the fuzzy tree are proposed. In the tests, variable levels of the fuzzy tree and the optimum results were achieved by using *three* levels of the fuzzy tree.

Step 2.1: Extract the histogram of the image.

Step 2.2: Divide the histogram into two parts.

$$H_1 = H(1:128) \quad (9)$$

$$H_2 = H(129:256) \quad (10)$$

where H is the histogram of the image, H_1 and H_2 parts of the histogram.

Step 2.3: Calculate indices of the maximum points of the H_1 and H_2 and these points are used to create triangle fuzzy sets. The pseudocode of this calculation is given in Fig. 5.

Procedure: Peak value calculation

Input: Histogram pieces, H_1 and H_2 with size of 128

Output: Threshold points, t_1 and t_2

01: Calculate maximum points of the pieces. $m_1 = \max(H_1)$, $m_2 = \max(H_2)$

02: **for** i=1 to 128 **do**

03: **if** $H_1(i) = m_1$ **then**

04: $t_1 = i$;

05: **end if**

06: **if** $H_2(i) = m_2$ **then**

07: $t_2 = i$;

08: **end if**

09: **end for**

10: $t_2 = t_2 + 128$;

Fig. 5. Pseudocode of the peak value (threshold value) calculation

Step 2.4: Create triangle fuzzy sets using t_1 and t_2. A and B sets are created using these points.

Step 2.5: Calculate membership degrees of each pixel using Eqs. 11-12.

$$\mu_A(pv) = \begin{cases} \dfrac{pv}{t_1}, & pv \le t_1 \\ \dfrac{255 - pv}{255 - t_1}, & pv > t_1 \end{cases} \quad (11)$$

$$\mu_B(pv) = \begin{cases} \dfrac{pv}{t_2}, & pv \le t_2 \\ \dfrac{255 - pv}{255 - t_2}, & pv > t_2 \end{cases} \quad (12)$$

where μ_A and μ_B represent membership degrees of the A and B sets, pv describes pixel value. By using these membership degrees, novel images are created. The procedure of the fuzzy tree-based image generation is given in Fig. 6.

Procedure: Fuzzy tree based image generation

Input: Image I with size of W x H

Output: Feature images FI with size of W x H x 15, k={1,2,3}

01: Load image I

02: count=1;

03: $[A\ B] = tft(I)$ // $tft(.)$ is triangle fuzzy transform

04: $FI^0 = I; FI_1^2 = A; FI_2^1 = B;$ // Assign images to FI

05: $[FI_1^2\ FI_2^2] = tft(A)$

06: $[FI_3^2\ FI_4^2] = tft(B)$

07: **for** i=1 to 4 **do**

08: $[FI_{count}^3\ FI_{count+1}^3] = tft(FI_i^2);$

09: $count = count + 2;$

10: **end for i**

Fig. 6. The fuzzy tree-based image generation

Step 3: Resize the generated 15 images to 256 x 256 sized images.

Step 4: Extract 768 features from each image by using MKLBP.

Step 5: Divide images into 128 x 128 sized exemplars.

Step 6: Extract 768 features from each exemplar.

Step 7: Concatenate the features and obtain a final feature vector with a size of 768 x 75=57,600.

Step 8: Apply INCA to extracted 57,600 features and select 616 most valuable features.

NCA [48] is one of the commonly preferred feature selection methods. It calculates positive weights for each feature. Firstly, NCA assigns a weight for each feature randomly. It calculates the correlation of the features and target by using a city block distance-based fitness function. By using stochastic gradient descent optimization, optimum weight values are set. The main problem of the NCA is the selection of the optimal number of features. Because the whole weights of the NCA are positive. Therefore, redundant features cannot be assigned, and feature selection is implemented parametrically. Iterative NCA is developed to solve this problem. In the INCA, a loss value calculator is also needed. So k-NN classifier with 10-fold cross-validation was used as a loss value calculator. The steps of the proposed INCA are shown below.

Step 8.1: Apply min-max normalization to extracted 57,600 features. Because NCA is a distance-based feature selector. Min-max normalization phase should be used to use effectiveness of the NCA [49].

$$X^N(:,i) = \frac{X(:,i) - X(:,i)_{min}}{X(:,i)_{max} - X(:,i)_{min}} \quad (13)$$

where $X(:,i)$ is i[th] feature and X^N denotes normalized features.

Step 8.2: Apply NCA weight generation function to normalized features.

$$[weights\ index] = NCA(X^N, target); \quad (14)$$

$index$ is the ordered indices of the sorting features by descending.

Step 8.3: Set an upper and lower range value to iteratively calculate loss value. The range is from 40 features to 1040 features.

Step 8.4: Select features.

$$fs^{t-39}(:,t) = X\big(:, index(t)\big), \quad t = \{1,2,\dots,40+g\}, \quad g = \{0,1,\dots,1000\} \quad (15)$$

fs^t is t[th] selected feature vector.

Step 8.5: Calculate the loss values of the selected feature vectors.

$$loss(h) = kNN(fs^h, target, 10, CB, 1) \quad (16)$$

where $loss$ is calculated loss value, kNN is k-NN [50] function, which is calculated loss value. Parameters of the loss function are the, features, target, k-fold validation (10-fold CV is selected), distance metric (CB represents city block) and k (k value is chosen as 1) value respectively.

Step 8.6: Find the minimum loss of valued features and indices of it.

$$[minimum\ indice] = min(loss) \quad (17)$$

Step 8.7: Select the minimum loss of valued features using Eq. 18.

$$fs^{final}(:,t) = X\big(:, endex(t)\big), \quad t = \{1,2,\dots,39+indice\} \quad (18)$$

where fs^{final} final selected feature vector.

Step 9: Use the final selected feature vector as the input of the selected 16 classifiers with 10-fold cross-validation. The details of the used classifiers are given in the experimental results section.

Further, the pseudocode of the presented F-transform and MKLBP based exemplar feature generation and INCA feature selection based model is also given below.

Algorithm 1. Psuedo code of the presented F-transform and MKLBP based exemplar feature generation and INCA selector based automated Covid19 detection model.

Input: Covid image dataset (DB) with a size of D (number of images). **Output:** Results
00: Load Covid19 chest image dataset. 01: **for** k=1 to D **do** 02: Read image (Im) 03: Apply F-transform based image generation (It is defined in Figure 6) 04: Obtain 15 F-transform images 05: Resize F-transformed images into 256 x 256 sized images. 06: Divide these images into exemplars with a size of 128 x 128. 07: Generate features from these images and original image using MKLBP. 08: Merge the extracted features and obtain feature vector with a length of 57,600. 09: **end for k** 10: Apply INCA to the extracted feature vector and select the most discriminative feaures. 11: Feed the chosen features to conventional classifiers and obtain results.

5. Experımental Results

In this section, the results of the proposed fuzzy MKLBP and INCA based approach are given. This method is implemented on MATLAB (2019b) programming environment. The used exemplar fuzzy MKLBP and INCA feature selection are coded on MATLAB M files. MATLAB Classification Learner Toolbox (MCLT) was used for classification. 16 classifiers in 5 groups were utilized as classification methods. These classifiers and their attributes were listed in Table 1. 616 features were forwarded to these classifiers.

Table 1. The parameters of the used classifiers

Group	**Classifier**	**Parameters**
Tree [51-53]	Fine	Number of splits: 100, Criteria: Gini
	Medium	Number of splits: 20, Criteria: Gini
Discriminant [54]	Linear Discriminant	Covariance structure is full.
SVM [55]	Cubic	Kernel: Cubic (3rd degree polynomial), C: 1, Multiclass: 1 vs 1
	Quadratic	Kernel: Quadratic (2nd degree polynomial), C: 1, Multiclass: 1 vs 1

	Gaussian	Kernel: Gaussian, C: 1, Multiclass: 1 vs 1
	Linear	Kernel: Linear, C: 1, Multiclass: 1 vs 1
k-NN [50]	Fine	k:1, Distance: City Block, Weight: Equal
	Medium	k:10, Distance: Euclidean, Weight: Equal
	Coarse	k:100, Distance: Euclidean, Weight: Equal
	Cosine	k:10, Distance: Cosine, Weight: Equal
	Cubic	k:10, Distance: Cubic, Weight: Equal
	Weighted	k:10, Weight: Squared inverse Distance: Euclidean,
Ensemble [56]	Bagged Tree	Method: Bag, Splits: 434, Learners: 30 Learner type: Decision tree,
	Subspace discriminant	Subspace domain: 308,Method: Subspace, Learners: 30, Learner type: Discriminant
	Subspace k-NN	Subspace domain: 308, Method: Subspace, Learners: 30, Learner type: k-NN,

In the literature, accuracy, geometric mean, Precision, and recall parameters have been widely used to evaluate models. Testing and training observations are selected randomly. Therefore, tests of each classifier were repeated 100 times to obtain general results. The obtained results were shown in Table 2, and mathematical notations of the used evaluation parameters were given as below [23, 57].

$$Accuracy = \frac{tps + tns}{tps + tns + fps + fns} \tag{19}$$

$$Recall = \frac{tps}{tps + fns} \tag{20}$$

$$Precision = \frac{tps}{tps + fps} \tag{21}$$

$$Geometric\ mean = \sqrt{\frac{tps * tns}{(tps + fns)(tns * fps)}} \tag{22}$$

where $tps, tns, fps,$ and fns are true positives, true negatives, false positives, and false negatives, respectively.

As it can be seen in Table 2, experimental studies on 16 classifiers were carried out. In each experiment, 10-fold cross-validation was used, and accuracy, geometric mean, Precision, and recall parameters were calculated. Maximum, minimum, mean, and standard deviation values of these parameters were obtained by running each classifier 100 times. When the results obtained in the experimental studies are examined, it is seen that the accuracy of the SVM

classifier is at the highest rates with 97.01% and 96.78% values. After these accuracy values, the Ensemble Subspace k-NN classifier has become the highest accuracy value of 96.55% ratio. The highest values in the study were obtained using the SVM Cubic classifier. The maximum accuracy rate of 97.01%, a minimum accuracy of 95.17%, an average accuracy of 96.23% were obtained with this classifier. The standard deviation is only 0.42%. The small standard deviation indicates that the results obtained with this classifier are close to each other. It is seen that these classifiers give the highest Geometric mean, Precision, and Recall values. The results obtained from the experimental results show that the proposed method is successful in diagnosing COVID-19.

Table 2. Performance results (%) of the used classifiers

Group	Classifiers	Statistical Evaluation	Accuracy	Geometric Mean	Precision	Recall
DT	Tree Fine	Max	86.90	87.00	86.97	87.06
		Mean	83.57	83.64	83.68	83.81
		Min	80.23	80.24	80.30	80.54
		Std	1.40	1.41	1.40	1.38
	Tree Medium	Max	86.90	86.98	86.94	87.16
		Mean	83.56	83.63	83.67	83.80
		Min	80.46	80.46	80.70	80.74
		Std	1.39	1.40	1.38	1.38
LD	LD	Max	82.30	82.12	82.46	82.86
		Mean	79.11	78.80	79.14	79.69
		Min	76.55	76.18	76.57	77.04
		Std	1.34	1.40	1.35	1.32
SVM	Cubic	Max	97.01	97.06	97.11	97.09
		Mean	96.23	96.29	96.37	96.32
		Min	95.17	95.22	95.34	95.26
		Std	0.42	0.43	0.40	0.43
	Quadratic	Max	96.78	96.83	96.90	96.86
		Mean	95.84	95.90	96.00	95.94
		Min	94.94	94.96	95.13	94.99
		Std	0.38	0.38	0.36	0.38
	Gaussian	Max	96.32	96.39	96.44	96.42
		Mean	95.37	95.46	95.50	95.50
		Min	94.02	94.09	94.15	94.15
		Std	0.44	0.44	0.43	0.43
	Linear	Max	95.40	95.48	95.57	95.53
		Mean	94.75	94.83	94.93	94.89
		Min	94.02	94.09	94.29	94.15
		Std	0.31	0.31	0.30	0.31
k-NN	Fine	Max	96.09	96.16	96.29	96.20
		Mean	95.19	95.24	95.42	95.28

		Min	93.10	93.12	93.51	93.14
		Std	0.59	0.60	0.55	0.60
	Medium	Max	93.33	93.39	93.68	93.41
		Mean	92.25	92.27	92.69	92.29
		Min	91.03	91.05	91.45	91.09
		Std	0.42	0.43	0.40	0.43
	Coarse	Max	87.13	86.92	88.02	87.06
		Mean	85.84	85.54	86.79	85.75
		Min	84.83	84.44	85.82	84.69
		Std	0.50	0.52	0.47	0.51
	Cosine	Max	92.64	92.73	92.81	92.81
		Mean	91.70	91.77	91.80	91.89
		Min	90.34	90.42	90.42	90.54
		Std	0.48	0.48	0.48	0.47
	Cubic	Max	92.87	92.87	93.31	92.89
		Mean	91.79	91.74	92.34	91.76
		Min	90.57	90.49	91.14	90.52
		Std	0.45	0.46	0.41	0.45
	Weighted	Max	95.86	95.92	96.05	95.95
		Mean	94.78	94.85	95.01	94.90
		Min	93.79	93.81	94.09	93.85
		Std	0.44	0.44	0.41	0.44
Ensemble	Bagged Tree	Max	93.10	93.21	93.12	93.31
		Mean	90.92	91.02	90.98	91.14
		Min	88.74	88.83	88.74	88.99
		Std	0.90	0.90	0.89	0.89
	Subspace Discriminant	Max	91.95	92.06	92.11	92.22
		Mean	89.87	89.94	90.03	90.18
		Min	87.36	87.42	87.63	87.70
		Std	1.08	1.09	1.06	1.05
	Subspace kNN	Max	96.55	96.59	96.73	96.62
		Mean	95.58	95.62	95.79	95.66
		Min	94.25	94.22	94.43	94.25
		Std	0.52	0.53	0.50	0.52

6. Discussions

The objective of this paper is to accurately classify chest X-ray images of the Covid-19, pneumonia, and healthy subjects. Our model consists of fuzzy image construction, exemplar MKLBP feature generation, and feature selection with INCA. These methods are explained in sections 2 and 4. The fuzzy tree is applied as a novel operator like convolution. In the feature generation phase, 57,600 features are extracted. INCA is applied to these features to select discriminative ones. INCA solves the automatic optimal feature selection problem of the NCA. A range of the number of features are defined to decrease computational cost. The plotting of the calculated loss values was also shown in Fig. 7.

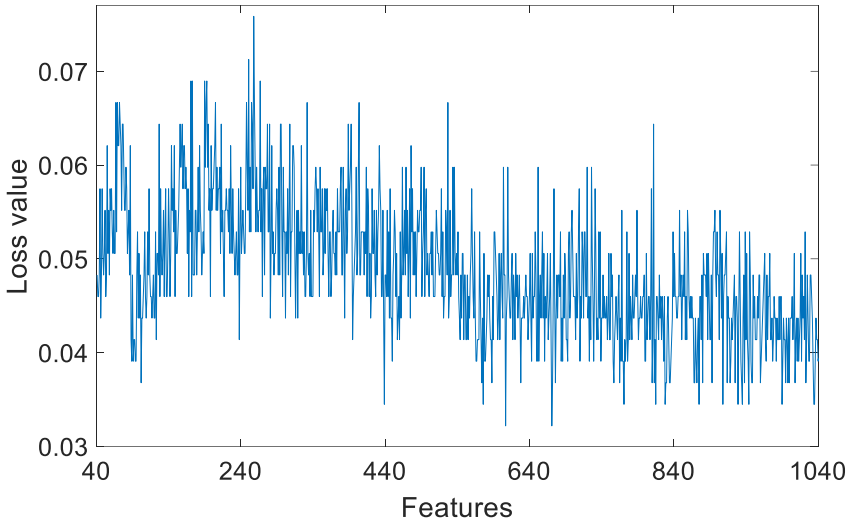

Fig.7. The calculated loss values of our feature by using INCA feature selector with Fine k-NN

Here, the k-NN classifier is used as a loss value (loss value=1-accuracy) generator. INCA is an iterative feature selector. Here, the initial and end iteration variables are selected as 40 and 1040. Hence, 1000 feature vectors are generated utilizing the iterative feature selection. The k-NN classifier is employed to the selected each feature vector in the iteration, and 1000 loss values are generated. The plot of the calculated loss values is denoted in Figure 7, and as seen in Figure 7, 616 features were selected by using INCA. These features were forwarded to 16 classifiers and results were listed (See Table 2). The presented F-transform and MKLBP generator and INCA selector model attained successful results on the used 16 shallow classifiers, and it is denoted the discriminative feature generation ability of the proposed approach. To show the discriminative ability of the created and selected features, statistical analysis (t-test) is applied to features of a couple of the classes. The boxplot of the generated p-values of the features of a couple of the classes p-values are shown in Figure 8.

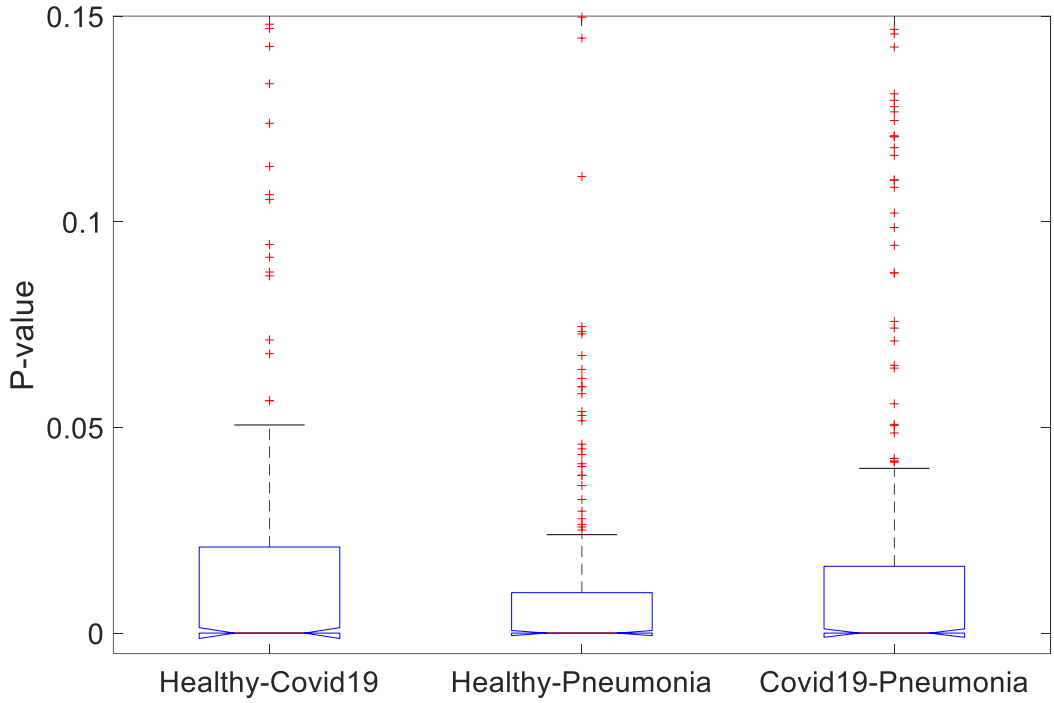

Fig. 8. Boxplot of the generated p-values of the features of a couple of the classes.

Moreover, the calculated p-values are listed in Table 3.

Table 3. The calculated minimum of p-values.

Classes	Healthy-Covid19	Healthy-Pneumonia	Covid19-Pneumonia
p-values	7.0569e-42	5.6981e-31	0

Table 3 demonstrates that p-value of the Covid19-Pneumonia is found as 0. The confusion matrix of the presented model (See Figure 9) was proved these results.

We also utilize the pre-trained convolutional neural networks, which are AlexNet [58], GoogLeNet [59], Residual Networks (ResNet18 ResNet50, ResNet101) [60], Visual Geometry Group Networks (VGG16, VGG19) [61], InceptionNet version 3 [62], DenseNet201 [63] and MobileNet [64]. These networks are utilized as feature extractors, and Cubic SVM (our best classifier) is utilized as a classifier. Comparatively, results were listed in Table 4.

Table 4 demonstrates that the proposed fuzzy MKLBP and INCA based chest X-ray image classification method has achieved better success rate than the pre-trained feature extraction techniques. Pre-trained feature extraction models are used with the SVM classifier,

and the good classification accuracies are obtained. Therefore, SVM is selected as a classifier for comparison, and their best results are listed in Table 4.

Table 4. Results of the transfer learning models and our presented F-transform, MKLBP, and INCA based model.

Method	**Accuracy**
AlexNet [58]	93.56
GoogLeNet [59]	93.79
ResNet18 [60]	94.71
ResNet50 [60]	95.17
ResNet101 [60]	94.94
VGG16 [61]	94.02
VGG19 [61]	95.63
InceptionNet v3 [62]	93.56
DenseNet201 [63]	95.86
MobileNet [64]	93.79
Our Method	97.01

Our study also compared with the COVID-19 detection and classification studies from X-ray images in literature so far. Table 5 shows the comparison of the previous studies in the literature to verify the validity of the proposed F-transform based method.

Table 5. Comparison of the proposed method with previous studies.

Study	**Attributes of dataset**	**Feature extraction and classification methods**	**Type of Images**	**Accuracy (%)**
[65]	125 COVID-19 500 Healthy 500 Pneumonia	DarkCovidNet	Xray Images	87.02
[66]	25 COVID-19 25 Healthy	COVIDX-Net	Xray Images	90.0

[67]	224 COVID-19 504 Healthy 700 Pneumonia	VGG-19	Xray Images	93.48
[68]	777 COVID-19 708 Healthy	DRE-Net	CT Images	86
[69]	25 COVID-19 25 Healthy	ResNet50þ SVM	Xray Images	95.38
[70]	313 COVID-19 229 Healthy	UNetþ3D Deep Network	CT Images	90.8
[46]	53 COVID-19 5526 Healthy	COVID-Net		92.4
[71]	219 COVID-19 175 Healthy 224 Pneumonia	ResNet þ Location Attention	CT Images	86.7
[30]	195 COVID-19 258 Healthy	M-Inception	CT Images	82.9
[72]	449 patients with COVID-19, 425 normal ones, 98 with lung cancer, 98 with lung cancer	Multitask learning	CT images	94.67
[73]	320 COVID-19 320 Healthy	Deep convolutional neural network	CT images	93.64
[74]	100 COVID-19 200 Healthy 322 Pneumonia	Convolutional neural network	Xray Images	95.74
[75]	80 COVID-19 72 Healthy 78 Pneumonia	Convolutional neural network	CT images	96.2
Our Proposed method	135 COVID-19, 150 Healthy 150 Pneumonia	F-transform, MKLBP and SVM	Xray Images	97.01

As seen in Table 5, deep learning models were used to obtain high performance on this problem. Our model uses a hand-crafted feature generator and an SVM classifier. The presented F-transform and MKLBP based image classification model attained 97.01% accuracy by using SVM classifier. The presented F-transform is utilized for both noise reduction and decomposition. By applying MKLBP, the salient features are generated, and INCA selects the most appropriate/discriminative features. Therefore, high classification rates are obtained using a conventional classifier. The developed method has shown that it can assist to expert radiologists in diagnosing COVID-19. However, the proposed method can be made more robust and accurate with the increase of COVID-19 data. The confusion matrix of our best result was also shown in Figure 9.

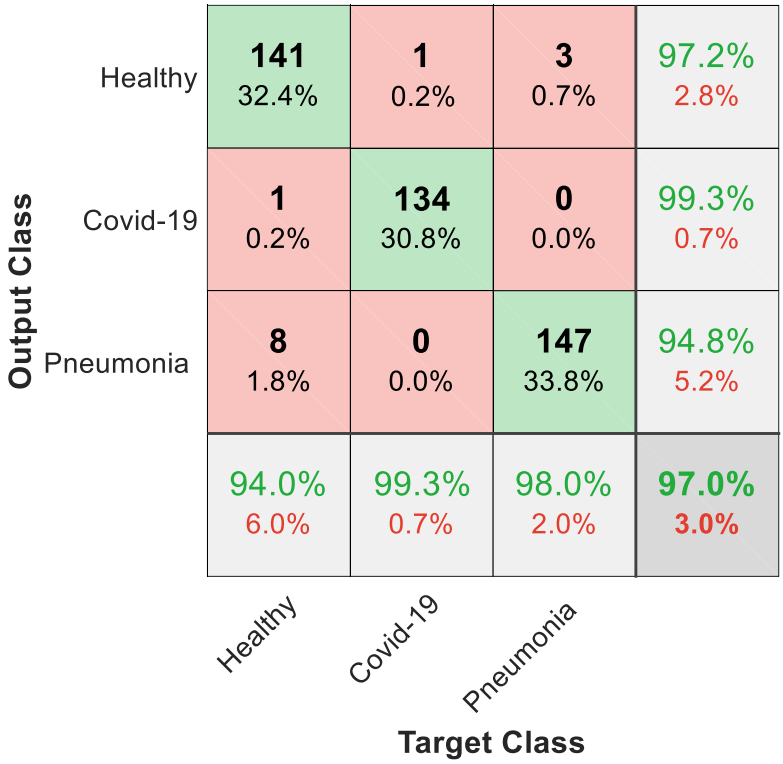

Fig. 9. Confusion matrix of our best result.

The benefits of the proposed fuzzy MKLBP and INCA based chest image classification method are given below.

- A novel fuzzy-based transformation is proposed similar to convolution.
- Normally, X-ray image patterns of Covid-19 and pneumonia diseases are similar. Therefore, these X-ray images are difficult to differentiate. The proposed fuzzy MKLBP and INCA based method classified these diseases successfully (See Fig. 8).
- A high accurate classification performance is achieved by the proposed approach.

- Comprehensive results are obtained by using 16 classifiers (See Table 2).
- The proposed approach is a cognitive method because there is no need to set millions of parameters as deep learning networks.
- The proposed approach has achieved higher classification accuracy than **ten** pre-trained deep learning networks (See Table 4).
- A small dataset is used with the presented model. Bigger datasets or more chest related disorders can be used.

7. Conclusions

The covid-19 pandemic has affected all of the world. Therefore, it has become one of the most important and hot-topic research area. To contribute Covid-19 researches, a novel automated chest X-ray image classification method is proposed. This method consists of fuzzy tree creation, exemplar MKLBP based feature extraction, INCA based feature selection, and classification procedures. By using the fuzzy tree, a novel F-transformation is proposed, and this transformation is used as an image operator, and 15 variable images are obtained from each chest X-ray image. MKLBP generates features from these chest X-ray images and exemplars of these images. INCA solves the automated optimal feature selection problem of the NCA. The obtained feature vector is tested on 16 classifiers with *five* groups. According to the results, Cubic SVM has achieved 97.01% classification accuracy. The obtained results are compared to the transfer learning based feature extraction model, and previous studies in Table 3 and 5. The presented results reveal that the proposed framework is successful for Covid-19 detection using chest X-ray images. Covid-19 and pneumonia show similar characteristics. Therefore, their chest X-ray images are similar. The proposed fuzzy MKLBP and INCA based approach has the ability of discrimination of these diseases successfully.

As a future work, a real time automated Covid-19 detection system can be created using the proposed MKLBP and fuzzy transform-based model. The architecture of our planned future is summarized in Figure 10.

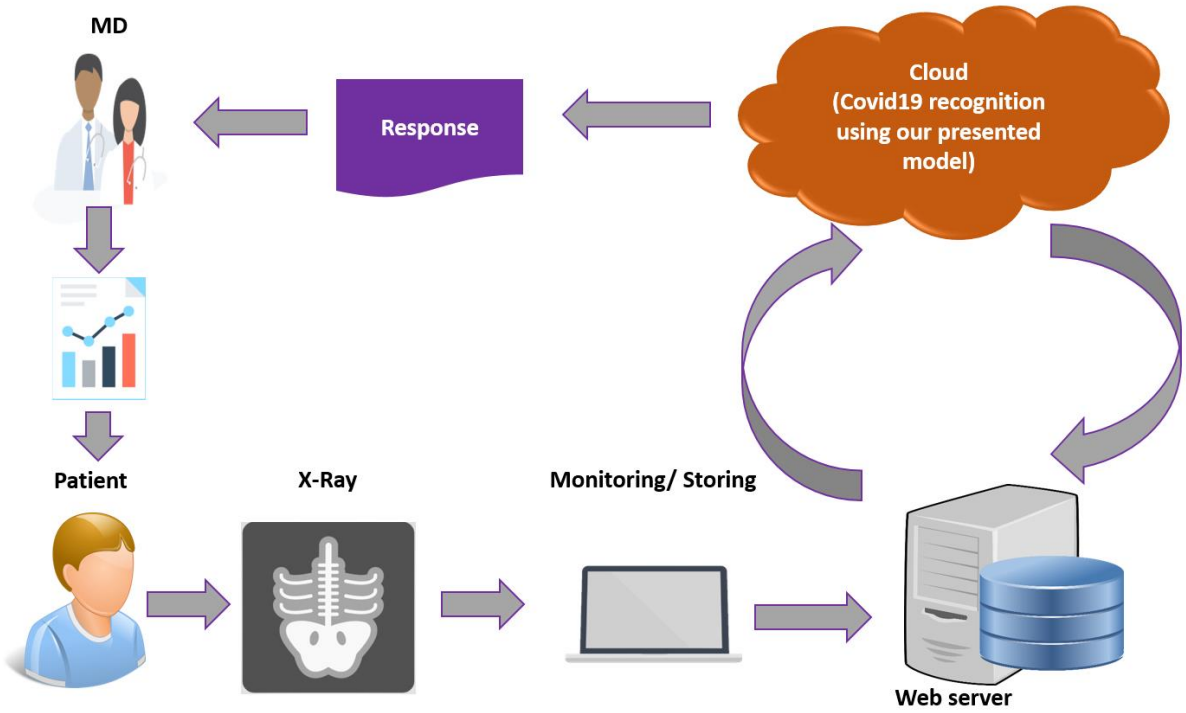

Fig. 10. Snapshot of the architecture of the intended/planned cloud-based automated Covid19 detection application.

Moreover, new generation binary pattern-based deep models and F-transform based decomposers can be recommended.

Funding

There is no funding source for this article.

Conflicts of interest

The authors declare that there is no conflict of interest related to this paper.

References

[1] H.A. Rothan, S.N. Byrareddy, The epidemiology and pathogenesis of coronavirus disease (COVID-19) outbreak, Journal of autoimmunity, (2020) 102433.

[2] P. Zhai, Y. Ding, X. Wu, J. Long, Y. Zhong, Y. Li, The epidemiology, diagnosis and treatment of COVID-19, International Journal of Antimicrobial Agents, (2020) 105955.

[3] A.J. Rodriguez-Morales, J.A. Cardona-Ospina, E. Gutiérrez-Ocampo, R. Villamizar-Peña, Y. Holguin-Rivera, J.P. Escalera-Antezana, L.E. Alvarado-Arnez, D.K. Bonilla-Aldana, C. Franco-Paredes, A.F. Henao-Martinez, Clinical, laboratory and imaging features of COVID-19: A systematic review and meta-analysis, Travel medicine and infectious disease, (2020) 101623.

[4] S. Chavez, B. Long, A. Koyfman, S.Y. Liang, Coronavirus Disease (COVID-19): A primer for emergency physicians, The American Journal of Emergency Medicine, (2020).
[5] Y.C. Li, W.Z. Bai, T. Hashikawa, The neuroinvasive potential of SARS-CoV2 may be at least partially responsible for the respiratory failure of COVID-19 patients, Journal of medical virology, (2020).
[6] C. Yeo, S. Kaushal, D. Yeo, Enteric involvement of coronaviruses: is faecal–oral transmission of SARS-CoV-2 possible?, The Lancet Gastroenterology & Hepatology, 5 (2020) 335-337.
[7] Y.M. Arabi, S. Murthy, S. Webb, COVID-19: a novel coronavirus and a novel challenge for critical care, Intensive care medicine, (2020) 1-4.
[8] M. Wieczorek, J. Siłka, M. Woźniak, Neural network powered COVID-19 spread forecasting model, Chaos, Solitons & Fractals, 140 (2020) 110203.
[9] M. Wieczorek, J. Siłka, D. Połap, M. Woźniak, R. Damaševičius, Real-time neural network based predictor for cov19 virus spread, Plos one, 15 (2020) e0243189.
[10] M. Woźniak, D. Połap, Bio-inspired methods modeled for respiratory disease detection from medical images, Swarm and evolutionary computation, 41 (2018) 69-96.
[11] Q. Ke, J. Zhang, W. Wei, D. Połap, M. Woźniak, L. Kośmider, R. Damaševĭcius, A neuro-heuristic approach for recognition of lung diseases from X-ray images, Expert Systems with Applications, 126 (2019) 218-232.
[12] C.A. Devaux, J.-M. Rolain, P. Colson, D. Raoult, New insights on the antiviral effects of chloroquine against coronavirus: what to expect for COVID-19?, International Journal of Antimicrobial Agents, (2020) 105938.
[13] K.-S. Yuen, Z.-W. Ye, S.-Y. Fung, C.-P. Chan, D.-Y. Jin, SARS-CoV-2 and COVID-19: The most important research questions, Cell & bioscience, 10 (2020) 1-5.
[14] K.J. Clerkin, J.A. Fried, J. Raikhelkar, G. Sayer, J.M. Griffin, A. Masoumi, S.S. Jain, D. Burkhoff, D. Kumaraiah, L. Rabbani, Coronavirus Disease 2019 (COVID-19) and Cardiovascular Disease, Circulation, (2020).
[15] L. Li, Z. Yang, Z. Dang, C. Meng, J. Huang, H. Meng, D. Wang, G. Chen, J. Zhang, H. Peng, Propagation analysis and prediction of the COVID-19, Infectious Disease Modelling, 5 (2020) 282-292.
[16] M.A. Shereen, S. Khan, A. Kazmi, N. Bashir, R. Siddique, COVID-19 infection: origin, transmission, and characteristics of human coronaviruses, Journal of Advanced Research, (2020).
[17] E. Aydemir, Weka ile yapay zeka, Seçkin Yayınevi, Ankara, (2018).

[18] E. Aydemir, S. Gulsecen, Arranging Bus Behaviour by Finding the Best Prediction Model with Artificial Neural Networks, Tehnički vjesnik, 26 (2019) 885-892.
[19] F.B. Demir, T. Tuncer, A.F. Kocamaz, A chaotic optimization method based on logistic-sine map for numerical function optimization, Neural Computing and Applications, (2020) 1-13.
[20] T. Tuncer, S. Dogan, F. Ozyurt, An automated Residual Exemplar Local Binary Pattern and iterative ReliefF based corona detection method using lung X-ray image, Chemometrics and Intelligent Laboratory Systems, (2020) 104054.
[21] F. Özyurt, Uzaktan Algılama Görüntülerinin Evrişimsel Sinir Ağları ve Komşuluk Bileşen Analizi Tabanlı Özniteliklerinin Sınıflandırılması, Afyon Kocatepe Üniversitesi Fen Ve Mühendislik Bilimleri Dergisi, 19 669-675.
[22] E. Sert, F. Özyurt, A. Doğantekin, A new approach for brain tumor diagnosis system: Single image super resolution based maximum fuzzy entropy segmentation and convolutional neural network, Medical hypotheses, 133 (2019) 109413.
[23] F.B. Demir, T. Tuncer, A.F. Kocamaz, F. Ertam, A survival classification method for hepatocellular carcinoma patients with chaotic Darcy optimization method based feature selection, Medical Hypotheses, 139 (2020) 109626.
[24] A. Narin, C. Kaya, Z. Pamuk, Automatic Detection of Coronavirus Disease (COVID-19) Using X-ray Images and Deep Convolutional Neural Networks, arXiv preprint arXiv:2003.10849, (2020).
[25] E. Olejarczyk, W. Jernajczyk, Graph-based analysis of brain connectivity in schizophrenia, PLoS One, 12 (2017) e0188629.
[26] A.K. Jaiswal, P. Tiwari, S. Kumar, D. Gupta, A. Khanna, J.J. Rodrigues, Identifying pneumonia in chest X-rays: A deep learning approach, Measurement, 145 (2019) 511-518.
[27] X. Wang, Y. Peng, L. Lu, Z. Lu, M. Bagheri, R.M. Summers, Chestx-ray8: Hospital-scale chest x-ray database and benchmarks on weakly-supervised classification and localization of common thorax diseases, Proceedings of the IEEE conference on computer vision and pattern recognition, 2017, pp. 2097-2106.
[28] P.K. Sethy, S.K. Behera, Detection of coronavirus Disease (COVID-19) based on Deep Features, (2020).
[29] X. Xu, X. Jiang, C. Ma, P. Du, X. Li, S. Lv, L. Yu, Y. Chen, J. Su, G. Lang, Deep learning system to screen coronavirus disease 2019 pneumonia, arXiv preprint arXiv:2002.09334, (2020).

[30] S. Wang, B. Kang, J. Ma, X. Zeng, M. Xiao, J. Guo, M. Cai, J. Yang, Y. Li, X. Meng, A deep learning algorithm using CT images to screen for Corona Virus Disease (COVID-19), MedRxiv, (2020).
[31] I. Sirazitdinov, M. Kholiavchenko, T. Mustafaev, Y. Yixuan, R. Kuleev, B. Ibragimov, Deep neural network ensemble for pneumonia localization from a large-scale chest x-ray database, Computers & Electrical Engineering, 78 (2019) 388-399.
[32] S.K. Prabhakar, H. Rajaguru, S.-W. Lee, A Framework for Schizophrenia EEG Signal Classification With Nature Inspired Optimization Algorithms, IEEE Access, 8 (2020) 39875-39897.
[33] G. Liang, L. Zheng, A transfer learning method with deep residual network for pediatric pneumonia diagnosis, Computer methods and programs in biomedicine, (2019) 104964.
[34] D. Kermany, K. Zhang, M. Goldbaum, Labeled optical coherence tomography (oct) and chest X-ray images for classification, Mendeley data, 2 (2018).
[35] P. Rajpurkar, J. Irvin, K. Zhu, B. Yang, H. Mehta, T. Duan, D. Ding, A. Bagul, C. Langlotz, K. Shpanskaya, Chexnet: Radiologist-level pneumonia detection on chest x-rays with deep learning, arXiv preprint arXiv:1711.05225, (2017).
[36] B. Ghoshal, A. Tucker, Estimating Uncertainty and Interpretability in Deep Learning for Coronavirus (COVID-19) Detection, arXiv preprint arXiv:2003.10769, (2020).
[37] J.P. Cohen, Open database of covid-19 cases (2020), https://github.com/ieee8023/covid-chestxray-dataset.
[38] T.D. Pham, Classification of COVID-19 chest X-rays with deep learning: new models or fine tuning?, Health Information Science and Systems, 9 (2021) 1-11.
[39] H. Sallay, S. Bourouis, N. Bouguila, Online Learning of Finite and Infinite Gamma Mixture Models for COVID-19 Detection in Medical Images, Computers, 10 (2021) 6.
[40] L. Sun, Z. Mo, F. Yan, L. Xia, F. Shan, Z. Ding, B. Song, W. Gao, W. Shao, F. Shi, Adaptive feature selection guided deep forest for covid-19 classification with chest ct, IEEE Journal of Biomedical and Health Informatics, 24 (2020) 2798-2805.
[41] I. Perfilieva, V. Novák, A. Dvořák, Fuzzy transform in the analysis of data, International Journal of Approximate Reasoning, 48 (2008) 36-46.
[42] F. Di Martino, P. Hurtik, I. Perfilieva, S. Sessa, A color image reduction based on fuzzy transforms, Information Sciences, 266 (2014) 101-111.
[43] T. Tuncer, S. Dogan, F. Özyurt, S.B. Belhaouari, H. Bensmail, Novel Multi Center and Threshold Ternary Pattern Based Method for Disease Detection Method Using Voice, IEEE Access, 8 (2020) 84532-84540.

[44] T. Ojala, M. Pietikäinen, T. Mäenpää, A generalized local binary pattern operator for multiresolution gray scale and rotation invariant texture classification, International Conference on Advances in Pattern Recognition, Springer, 2001, pp. 399-408.
[45] X. Tan, B. Triggs, Enhanced local texture feature sets for face recognition under difficult lighting conditions, International workshop on analysis and modeling of faces and gestures, Springer, 2007, pp. 168-182.
[46] L. Wang, A. Wong, COVID-Net: A tailored deep convolutional neural network design for detection of COVID-19 cases from chest radiography images, arXiv preprint arXiv:2003.09871, (2020).
[47] M. Robnik-Šikonja, I. Kononenko, Theoretical and empirical analysis of ReliefF and RReliefF, Machine learning, 53 (2003) 23-69.
[48] S. Raghu, N. Sriraam, Classification of focal and non-focal EEG signals using neighborhood component analysis and machine learning algorithms, Expert Systems with Applications, 113 (2018) 18-32.
[49] Y.K. Jain, S.K. Bhandare, Min max normalization based data perturbation method for privacy protection, International Journal of Computer & Communication Technology, 2 (2011) 45-50.
[50] Q. Hu, D. Yu, Z. Xie, Neighborhood classifiers, Expert systems with applications, 34 (2008) 866-876.
[51] S.R. Safavian, D. Landgrebe, A survey of decision tree classifier methodology, IEEE transactions on systems, man, and cybernetics, 21 (1991) 660-674.
[52] K. Polat, S. Güneş, Classification of epileptiform EEG using a hybrid system based on decision tree classifier and fast Fourier transform, Applied Mathematics and Computation, 187 (2007) 1017-1026.
[53] R. Fournier, R. Landry, N. August, G. Fedosejevs, R. Gauthier, Modelling light obstruction in three conifer forests using hemispherical photography and fine tree architecture, Agricultural and Forest Meteorology, 82 (1996) 47-72.
[54] S. Chen, X. Yang, Alternative linear discriminant classifier, Pattern Recognition, 37 (2004) 1545-1547.
[55] K. Lau, Q. Wu, Online training of support vector classifier, Pattern Recognition, 36 (2003) 1913-1920.
[56] J.J. Rodriguez, L.I. Kuncheva, C.J. Alonso, Rotation forest: A new classifier ensemble method, IEEE transactions on pattern analysis and machine intelligence, 28 (2006) 1619-1630.

[57] T. Tuncer, S. Dogan, P. Pławiak, U.R. Acharya, Automated arrhythmia detection using novel hexadecimal local pattern and multilevel wavelet transform with ECG signals, Knowledge-Based Systems, 186 (2019) 104923.
[58] A. Krizhevsky, I. Sutskever, G.E. Hinton, Imagenet classification with deep convolutional neural networks, Advances in neural information processing systems, 2012, pp. 1097-1105.
[59] C. Szegedy, W. Liu, Y. Jia, P. Sermanet, S. Reed, D. Anguelov, D. Erhan, V. Vanhoucke, A. Rabinovich, Going deeper with convolutions, Proceedings of the IEEE conference on computer vision and pattern recognition, 2015, pp. 1-9.
[60] K. He, X. Zhang, S. Ren, J. Sun, Deep residual learning for image recognition, Proceedings of the IEEE conference on computer vision and pattern recognition, 2016, pp. 770-778.
[61] K. Simonyan, A. Zisserman, Very deep convolutional networks for large-scale image recognition, arXiv preprint arXiv:1409.1556, (2014).
[62] C. Szegedy, V. Vanhoucke, S. Ioffe, J. Shlens, Z. Wojna, Rethinking the inception architecture for computer vision, Proceedings of the IEEE conference on computer vision and pattern recognition, 2016, pp. 2818-2826.
[63] G. Huang, Z. Liu, L. Van Der Maaten, K.Q. Weinberger, Densely connected convolutional networks, Proceedings of the IEEE conference on computer vision and pattern recognition, 2017, pp. 4700-4708.
[64] A.G. Howard, M. Zhu, B. Chen, D. Kalenichenko, W. Wang, T. Weyand, M. Andreetto, H. Adam, Mobilenets: Efficient convolutional neural networks for mobile vision applications, arXiv preprint arXiv:1704.04861, (2017).
[65] T. Ozturk, M. Talo, E.A. Yildirim, U.B. Baloglu, O. Yildirim, U.R. Acharya, Automated detection of COVID-19 cases using deep neural networks with X-ray images, Computers in Biology and Medicine, (2020) 103792.
[66] E.E.-D. Hemdan, M.A. Shouman, M.E. Karar, Covidx-net: A framework of deep learning classifiers to diagnose covid-19 in x-ray images, arXiv preprint arXiv:2003.11055, (2020).
[67] I.D. Apostolopoulos, T.A. Mpesiana, Covid-19: automatic detection from x-ray images utilizing transfer learning with convolutional neural networks, Physical and Engineering Sciences in Medicine, (2020) 1.
[68] Y. Song, S. Zheng, L. Li, X. Zhang, X. Zhang, Z. Huang, J. Chen, H. Zhao, Y. Jie, R. Wang, Deep learning enables accurate diagnosis of novel coronavirus (COVID-19) with CT images, medRxiv, (2020).
[69] P.K. Sethy, S.K. Behera, Detection of coronavirus disease (covid-19) based on deep features, Preprints, 2020030300 (2020) 2020.

[70] C. Zheng, X. Deng, Q. Fu, Q. Zhou, J. Feng, H. Ma, W. Liu, X. Wang, Deep learning-based detection for COVID-19 from chest CT using weak label, medRxiv, (2020).
[71] C. Butt, J. Gill, D. Chun, B.A. Babu, Deep learning system to screen coronavirus disease 2019 pneumonia, Applied Intelligence, (2020) 1.
[72] A. Amyar, R. Modzelewski, H. Li, S. Ruan, Multi-task deep learning based CT imaging analysis for COVID-19 pneumonia: Classification and segmentation, Computers in Biology and Medicine, 126 (2020) 104037.
[73] Y.-D. Zhang, S.C. Satapathy, S. Liu, G.-R. Li, A five-layer deep convolutional neural network with stochastic pooling for chest CT-based COVID-19 diagnosis, Machine Vision and Applications, 32 (2021) 1-13.
[74] M.A. Zaki, S. Narejo, S. Zai, U. Zaki, Z. Altaf, N. u Din, Detection of nCoV-19 from Hybrid Dataset of CXR Images using Deep Convolutional Neural Network.
[75] S. Hu, Y. Gao, Z. Niu, Y. Jiang, L. Li, X. Xiao, M. Wang, E.F. Fang, W. Menpes-Smith, J. Xia, Weakly supervised deep learning for covid-19 infection detection and classification from ct images, IEEE Access, 8 (2020) 118869-118883.